Professor F. Garcia-Moliner, Professor L. Kadanoff, Professor R. J. Maurer, and Professor W. D. Compton. Dr. R. Candall helped on numerous occasions especially in connection with sample preparation and F to F' conversion. Dr. K. Kanazawa, Dr. R. Swank, and Dr. F. Lüty contributed to various aspects of the experiment and its interpretation. Dr. R. Tucker of Corning Glass Corporation kindly supplied some samples of electrically conducting glass. Thanks are also due to Dr. T. M. Srinivasan and Professor M. V. Klein for supplying certain crystals. One of the authors (RKA) was the recipient of fellowships from the National Science Foundation and the General Atomics Corporation. These are gratefully acknowledged.

PHYSICAL REVIEW VOLUME 136, NUMBER 1A 5 OCTOBER 1964

Paramagnetic Resonance of Fe^{3+} and Gd^{3+} in Yttrium Orthoaluminate*

R. L. WHITE
Stanford Electronics Laboratories, Stanford University, Stanford, California

G. F. HERRMANN
Lockheed Research Laboratories, Palo Alto, California

J. W. CARSON
Aerospace Group, Hughes Aircraft Company, Culver City, California

AND

M. MANDEL
Genetics Department, School of Medicine, Stanford University, Stanford, California

(Received 30 March 1964; revised manuscript received 4 June 1964)

The paramagnetic-resonance spectra of Fe^{3+} and Gd^{3+} in yttrium orthoaluminate were measured as part of an effort directed at understanding the isomorphic orthoferrites. The low symmetry of the ion sites and the complicated nature of the spectra necessitated the development of a special method of analysis for obtaining the relevant spin Hamiltonians. The method consisted of constructing directly from the angular dependence of the data "anisotropy surfaces," classical counterparts of the spin Hamiltonian, from which the spin Hamiltonian itself could be extracted by the method of operator equivalents. The predominant term in both Fe^{3+} and Gd^{3+} Hamiltonians was quadratic in the spin components. The fourth-order term of the Fe^{3+} Hamiltonian manifested very nearly cubic symmetry with the biquadratic coefficient a negative, contrary to general expectations. The Gd^{3+} spin Hamiltonian displayed no visible cubicity in the fourth-order terms. The "preferred" spin directions as determined in the orthoaluminate were compared with the observed spin configurations in the orthoferrites, and with the predictions of crystal-field calculations based on the ion position parameters of $GdFeO_3$. Correlation was very poor in both instances. No conclusive explanation of the discrepancies is at present available; the most likely explanation involved differences in the local crystal distortions between the orthoaluminate and the orthoferrite.

I. INTRODUCTION

IN recent years a great deal of progress has been made in understanding the magnetic properties of several classes of magnetic insulators on an atomic basis. Among experimental tools, paramagnetic resonance has been the chief instrument for investigating the individual magnetic ions (as opposed to the collective behavior observed in macroscopic studies), such studies being made, as a rule, in dilutely doped isomorphic nonmagnetic crystals, where the single-ion interactions can be observed separately from exchange.

Yttrium orthoaluminate, a nonmagnetic crystal, is of particular interest as a host for paramagnetic ions because of its crystallographic similarity to the important and relatively poorly understood class of magnetic materials—the orthoferrites. These are a family of mixed oxides of composition ABO_3 which crystallize in a slightly distorted perovskite form.[1–8] A is typically a trivalent rare earth and B a trivalent transition metal, though variations (involving, say, Ca or Ba substitutes) have been studied.[9–13] The magnetic sites in the ortho-

* The investigation reported here was performed for the greatest part at the Palo Alto Laboratories of the General Telephone and Electronics Corporation and was sponsored in part by the U. S. Air Force Cambridge Research Laboratories, Office of Aerospace Research, under contract No. AF 19(628)-387.

[1] S. Geller and E. A. Wood, Acta Cryst. **9**, 563 (1956).
[2] S. Geller and V. B. Bala, Acta Cryst. **9**, 1019 (1956).
[3] M. A. Gilleo, Acta Cryst. **10**, 161 (1957).
[4] S. Geller, Acta Cryst. **10**, 243 (1957).
[5] S. Geller, Acta Cryst. **10**, 248 (1957).
[6] S. Geller, J. Chem. Phys. **24**, 1236 (1956).
[7] S. Geller, Acta Cryst. **9**, 885 (1956).
[8] F. Bertaut and F. Forrat, J. Phys. Radium **17**, 129 (1956).
[9] E. O. Wollan and W. C. Koehler, Phys. Rev. **100**, 545 (1955).
[10] J. B. Goodenough, Phys. Rev. **100**, 564 (1955).
[11] U. H. Bents, Phys. Rev. **106**, 225 (1957).
[12] W. C. Koehler and E. O. Wollan, Chem. Phys. Solids **2**, 100 (1957).
[13] W. C. Koehler, E. O. Wollan, and M. K. Wilkinson, Phys. Rev. **118**, 58 (1960).

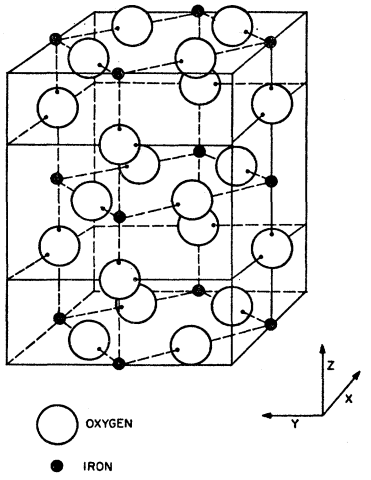

FIG. 1. Unit cell of the orthorhombic orthoferrite, showing idealized oxygen and iron sites. In actual crystal oxygen ions are slightly displaced from positions shown.

ferrites (and the corresponding sites in yttrium orthoaluminate) are distinguished by their low symmetry, which makes the theoretical treatment of the paramagnetic spectrum rather difficult. On the other hand, as first pointed out by Dzialoshinski,[14] it is this low symmetry which accounts for the manifestation on a macroscopic scale of the more interesting peculiarities of the orthoferrites such as canting, residual magnetism, and the spontaneous spin flipping at low temperature from one magnetic configuration into a different one.[15]

The over-all magnetic behavior of the orthoferrites is a composite result of single-ion mechanisms and exchange interactions.[16] The purpose of the present paramagnetic resonance measurements was the separate study of the magnetic environment of the single ion and in particular the crystalline anisotropy in these types of ion sites. The host crystal, yttrium orthoaluminate, was chosen in order to conform as closely as possible to the orthoferrite structure. Attempts to synthesize yttrium orthogalliate which was believed to afford a closer correspondence failed, and there is evidence that the compound does not exist.[4] The magnetic ions studied, both having as their ground state an $L=0$ (S) state, were Fe^{3+} substituting for Al^{3+} and Gd^{3+} substituting for Y^{3+}.

The analysis of the spectra presented unusual difficulties because of the lack of symmetry. It became evident that the customary procedure of fitting by trial and error to a spin Hamiltonian with adjustable parameters was impracticable in this case. The method which was eventually evolved consists in deriving so-called "anisotropy surfaces" directly from the data by employing certain sum rules based on a second-order perturbation formalism. The surfaces are fitted to potential functions which, in turn, yield the spin Hamiltonian by the method of operator equivalents. The procedure, described in Sec. IV, resulted in an accurate and detailed determination of the magnetocrystalline anisotropy for both Fe^{3+} and Gd^{3+} ions.

[14] I. Dzialoshinski, Phys. Chem. Solids 4, 241 (1958).
[15] R. M. Bozorth, Phys. Rev. Letters 1, 362 (1958).
[16] D. Treves, Phys. Rev. 125, 1843 (1962).

II. THE CRYSTAL STRUCTURE

The rare-earth orthoferrites and most of the rare-earth orthoaluminates, orthogalliates, orthochromites, etc., crystallize in an orthorhombically distorted perovskite structure. These compounds have been studied in considerable detail by Geller[1–7] and associates in this country and by Bertaut[8] and associates in France. We have unit cell dimensions for a wide range of A–B combinations but, at present, detailed information, e.g., exact oxygen positions, only for gadolinium orthoferrite.[6]

These materials belong to the orthorhombic space group D_{2h}^{16}—$Pbnm$. There are four distorted perovskite pseudocells in an orthorhombic unit cell, giving four distinct iron (aluminum) sites and four distinct rare-earth sites per unit cell. There are excellent visual presentations in the literature[1–7] and for our purposes a few schematic diagrams will suffice. The orthorhombic unit cell is drawn in Fig. 1. The rare-earth ions have been omitted from Fig. 1 to simplify the picture. They are shown separately in Fig. 2. The iron positions are special positions $(\frac{1}{2},0,0;\ \frac{1}{2},0,\frac{1}{2};\ 0,\frac{1}{2},0;\ 0,\frac{1}{2},\frac{1}{2})$, but all oxygen and rare-earth ions are displaced by as much as a few tenths of an angstrom from the idealized sites of Figs. 1 and 2. The iron site has only the inversion symmetry; the rare-earth site has mirror plane symmetry in the c planes.

III. EXPERIMENTAL PROCEDURES

The paramagnetic-resonance data were taken on a 35 kMc/sec superheterodyne magnetic-resonance spectrometer. Most of the data were taken at liquid-nitrogen temperatures, but some data were taken at 4.2°K, primarily to determine the sign of various Hamiltonian parameters. The sample crystals, approximately 1 mm on a side, and containing approximately 0.5 at.% of the magnetic ion, were mounted in the de-

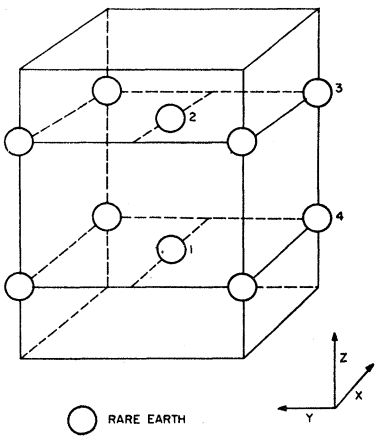

FIG. 2. Unit cell of the orthorhombic orthoferrite showing idealized positions of rare-earth ion sites.

sired orientation on a fixed probe and the electromagnet rotated to give the spectra in a plane.

A. The Fe^{3+} Spectra

The Fe^{3+} ion has $S=\frac{5}{2}$, and therefore gives rise to five transitions (of $\Delta M_z=1$ type) per ion. Since there are four magnetically inequivalent sites the spectrum consists of 20 absorptions for a general orientation of the external magnetic field H. For H in the principal planes of the crystal (e.g., the a–b plane) the number of magnetically inequivalent sites is reduced to two, and for H along the a, b or c directions, to one.

The low symmetry (inversion only) of the Fe^{3+} site gives us no *a priori* information as to the orientation of the principal axes of the crystal-field distortions, and indeed no guarantee that there will be any simple relationships between the principal axes of the quadratic potential and those of the biquadratic (fourth-power) potential. We are forced to determine these parameters entirely from the data.

The paramagnetic-resonance absorption spectrum of the Fe^{3+} ion in $YAlO_3$ was first recorded for H in the a–b plane and for H in the b–c plane. These data are presented in Figs. 3 and 4. It is not obvious from these data that any principal axes of the anisotropy surface were intercepted. However, the extremal spacings of the outermost transitions at about 25° from the b axis in the a–b plane, and the near symmetry in the spacings of a group of five lines at this orientation (the five transitions identified as belonging to sites 1 and 2 in Fig. 3), suggested that this direction was nearly a principal direction of the dominant perturbation. We expected the dominant perturbation to be quadratic in the spin components, as is usually the case for the Fe^{3+} spectrum. We therefore took data with H in a plane containing the c axis and the extremum in the a–b plane. These data showed that the extremum was located in, or within two or three degrees of, the a–b plane. Concluding then that this direction, 25° from b in the a–b plane, was a principal axis of the quadratic energy tensor, we took data with H in the plane perpendicular to this direction (henceforth called the "special plane") and obtained the spectrum shown in Fig. 5.

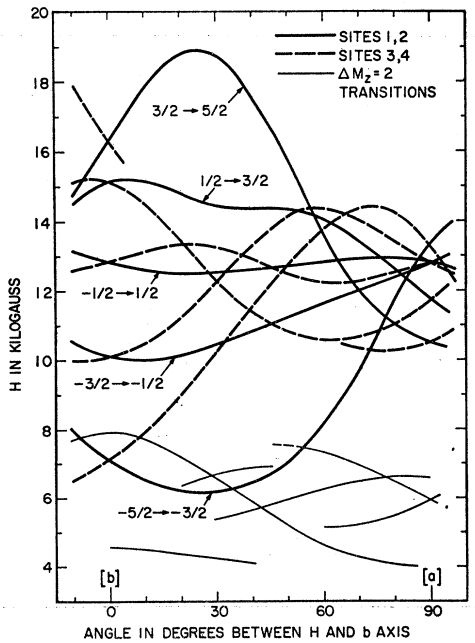

FIG. 3. Paramagnetic resonance absorption spectrums of Fe^{3+} in $YAlO_3$, with H in the a–b plane.

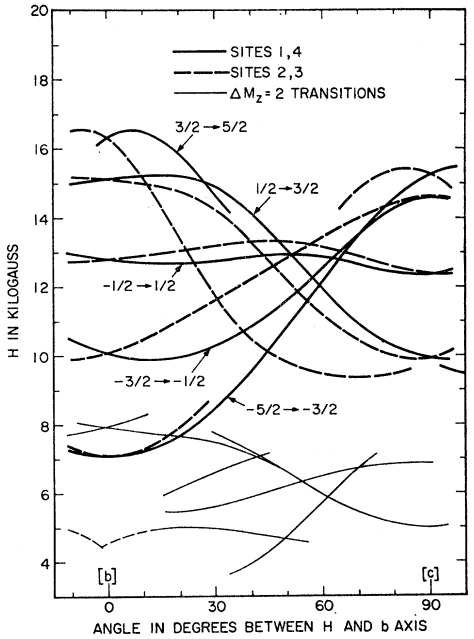

FIG. 4. Paramagnetic resonance absorption spectrum of Fe^{3+} in $YAlO_3$, with H in the b–c plane.

B. The Gd^{3+} Spectra

The rare-earth ion site in the orthoferrite is in a mirror plane perpendicular to the c axis. Therefore one principal axis of the relevant potential will always be the c axis, and the other axes are confined to the a–b plane. Further, the rare-earth sites are coupled in pairs by an inversion through the iron sites, so there are only two magnetically inequivalent rare-earth sites for any orientation of H. For H in the b–c or a–c planes the four sites are all magnetically equivalent. The Gd^{3+} spectrum is therefore relatively more simple than the Fe^{3+} spectrum, even though there is a larger number of transitions per site (seven transitions of $\Delta M_z=\pm 1$) because of the larger spin, $S=\frac{7}{2}$, of the Gd^{3+} ion.

The paramagnetic-resonance absorption spectrum of Gd^{3+} with H in the a–b plane is plotted in Fig. 6. The absorption spectrum with H in the b–c plane is plotted in Fig. 7. All necessary information is contained in these two spectra.

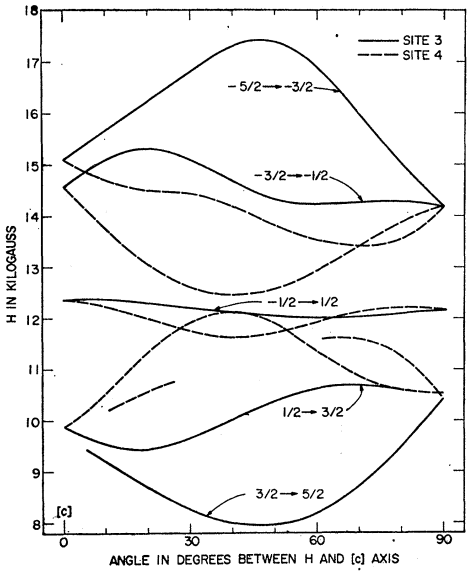

FIG. 5. Paramagnetic resonance absorption spectrum of Fe^{3+} in $YAlO_3$, with H in special plane (see text).

IV. METHOD OF ANALYSIS OF THE SPECTRA

The paramagnetic spectrum is described in terms of a spin Hamiltonian of the general form

$$\mathcal{H}=g\beta\mathbf{H}\cdot\mathbf{S}+\mathcal{H}_a(\mathbf{S}). \quad (1)$$

The first term is the Zeeman energy of interaction with an external field. Since both Fe^{3+} and Gd^{3+} are in a ground S state, the g factor can be assumed isotropic (the method described below can, however, be generalized to treat anisotropic g factors, too). $\mathcal{H}_a$ represents the anisotropy energy and is usually in the form of a polynomial in the components of $\mathbf{S}$.

The fitting of the spin Hamiltonian for a spin $\frac{5}{2}$ or $\frac{7}{2}$ ion to experimental data for a low-symmetry site presents a formidable problem. The most general form of a spin Hamiltonian for Fe^{3+} ions contains 14 adjustable parameters, that for Gd^{3+}, 15. Each guess at these parameters leads to a 6×6 or 8×8 matrix respectively, for each value and orientation of $\mathbf{H}$. Even with the use of perturbation methods the required labor is prohibitive.

The method to be described below bypasses these difficulties by deriving an approximate form for the Hamiltonian directly from the resonance data. This is accomplished by extensive use of the following well-known properties of "operator equivalents"[17–23]:

(1) For a given value of S, one can assign to any classical potential (harmonic) function a corresponding operator equivalent. Conversely, an operator $\mathcal{H}_a(\mathbf{S})$ can always be written in the form of the operator equivalent of a classical counterpart $\mathcal{H}_a(\boldsymbol{\alpha})$, which is the form that $\mathcal{H}_a(\mathbf{S})$ would take in the correspondence limit that $S\rightarrow\infty$ and becomes a classical vector which can be described entirely by its direction cosines. This classical potential $\mathcal{H}_a(\boldsymbol{\alpha})$ represents the dependence of the energy of the system upon the orientation of the magnetization, and appears regularly in ferromagnetic problems as an "anisotropy energy surface."

(2) Linear relations and transformation laws among operator equivalents are the same as among the classical counterparts.

Our approach will consist in determining the angular dependence of this classical potential $\mathcal{H}_a(\boldsymbol{\alpha})$ directly from the spectrum. The form of the spin Hamiltonian can then be determined by replacing each term in the classical potential by its appropriate operator equivalent.

The extraction of $\mathcal{H}_a(\boldsymbol{\alpha})$ from the data proceeds by utilizing two facts:

(1) The angular dependence of the diagonal elements of the spin Hamiltonian contains all the information required in order to determine the complete form of the potential.

(2) The experimental data can be processed in such a way as to obtain a direct determination (to 2nd order in perturbation theory) of the diagonal elements of the spin Hamiltonian.

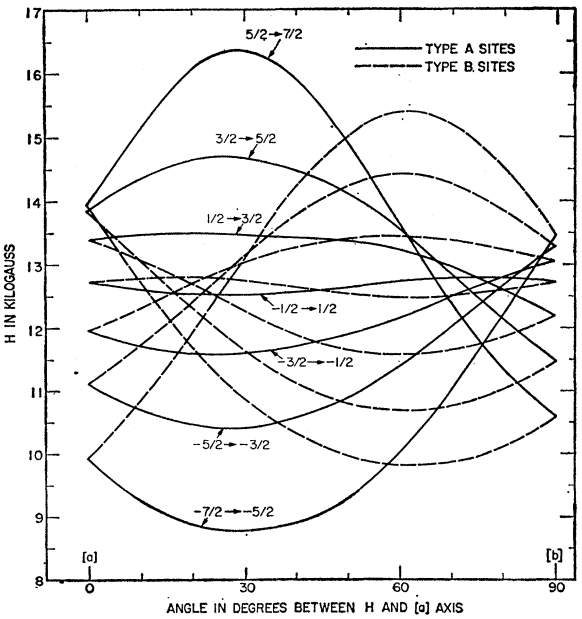

FIG. 6. Paramagnetic resonance absorption spectrum of Gd^{3+} in $YAlO_3$, with H in the a–b plane.

[17] K. W. H. Stevens, Proc. Phys. Soc. (London) **A65**, 209 (1952).
[18] R. J. Elliott and K. W. H. Stevens, Proc. Roy. Soc. (London) **A218**, 553 (1953).
[19] B. R. Judd, Proc. Roy. Soc. (London) **A227**, 552 (1955).
[20] R. J. Elliott and K. W. H. Stevens, Proc. Roy. Soc. (London) **A219**, 387 (1953).
[21] R. J. Elliott and K. W. H. Stevens, Proc. Phys. Soc. (London) **A64**, 205 (1951); **A64**, 832 (1951); **A65**, 370 (1952).
[22] W. Low, *Paramagnetic Resonance in Solids* (Academic Press Inc., New York, 1960), especially Chap. II.
[23] J. M. Baker, B. Bleaney, and W. Hayes, Proc. Roy. Soc. (London) **A247**, 141 (1958).

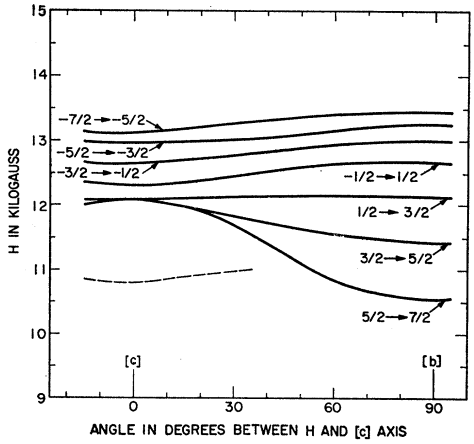

FIG. 7. Paramagnetic resonance absorption spectrum of Gd^{3+} in $YAlO_3$, with H in the b–c plane.

We start by expanding $\mathcal{H}_a$ in the form

$$\mathcal{H}_a(\mathbf{S})=g\beta\sum_l \bar{V}_l(S_1,S_2,S_3)\,, \tag{2}$$

where the coordinate axes denoted (1,2,3) are fixed with respect to a given site, and where summation is over even values of l for $2\leq l\leq 2S$. Each term $\bar{V}_l(\mathbf{S})$ is a polynomial of order l in the spin components S_1, S_2, S_3 and is the operator equivalent (in the following we shall consistently use bars to denote operator equivalents) of some classical potential $V_l(\alpha_1,\alpha_2,\alpha_3)$ which is a harmonic polynomial of order l in the components (direction cosines) of the unit vector $\boldsymbol{\alpha}$. Thus $V_l(\boldsymbol{\alpha})$ is one component of the "classical" $\mathcal{H}_a(\boldsymbol{\alpha})$ to which we alluded above. Each "anisotropy surface" $V_l(\boldsymbol{\alpha})$ can be written as some linear combination of the $2l+1$ spherical harmonics (or Kubic harmonics) of order l; and each $V_l(\boldsymbol{\alpha})$ therefore contains $2l+1$ expansion coefficients which are the parameters to be determined from the data.

The analysis relating the $V_l(\boldsymbol{\alpha})$ to the data proceeds initially along conventional lines. We first introduce a new coordinate system (x,y,z) with z along H. Next, we quantize the system with respect to the z direction, and, regarding $\mathcal{H}_a$ as a perturbation, write the energies of the system correct up to the 2nd-order terms in $\mathcal{H}_a$.

$$W(M_s)=g\beta HM_s+\langle M_s|\mathcal{H}_a|M_s\rangle + \sum_{M_s'\neq M_s}\frac{|\langle M_s|\mathcal{H}_a|M_s'\rangle|^2}{g\beta H_0(M_s-M_s')}, \tag{3}$$

where M_s represents, as usual, the eigenvalues of S_z. Equation (3) differs slightly from the standard form in that $H_0(=\hbar\nu/g\beta$, where ν is the fixed operating frequency) has been substituted for H in the denominator of the 2nd-order term. It can be shown that this change in fact represents a slight improvement in the approximation when we are required to fit data from the usual fixed frequency—variable magnetic-field resonance experiment.

Consider first the diagonal term

$$\langle M_s|\mathcal{H}_a|M_s\rangle=g\beta\sum_l\langle M_s|\bar{V}_l(\mathbf{S})|M_s\rangle. \tag{4}$$

To determine this element we first expand the corresponding "classical" potential at the ion site $V_l(\boldsymbol{\alpha})$ in terms of spherical harmonics defined relative to the (x,y,z) system:

$$V_l(\boldsymbol{\alpha})=\sum_{m=-l}^{+l}A_l^m(\mathbf{h})Y_l^m(x,y,z)\,, \tag{5}$$

where x, y, z are the components of $\boldsymbol{\alpha}$ in the (x,y,z) frame, and $\mathbf{h}=\mathbf{H}/|H|$ is a unit vector specifying the direction of $\mathbf{H}$ (and z) in the (1,2,3) coordinate frame. The functions Y_l^m are defined by

$$Y_l^{\pm m}=N_{lm}(x\pm iy)^m(d^m/dz^m)P_l(z)\,,$$

where P_l is a Legendre polynomial, N_{lm} is a normalization factor, and $m\geq 0$. The coefficients A_l^m depend, apart from a phase factor, only on the orientation of $\mathbf{H}$. The "operator equivalent" of the classical potential (5) is given by

$$V_l(\mathbf{S})=\sum_{m=-l}^{+l}A_l^m(\mathbf{h})\bar{Y}_l^m(S_x,S_y,S_z). \tag{6}$$

The operator equivalents of the Y_l^m have been tabulated[22,23] for $l\leq 6$, as have many of the matrix elements $\langle M_s'|\bar{Y}_l^m(\mathbf{S})|M_s\rangle$, and in particular we know that

$$\langle M_s'|\bar{Y}_l^m(\mathbf{S})|M_s\rangle=0, \quad \text{if } m\neq 0, \tag{7}$$

i.e., that we have diagonal elements only if $m=0$. To evaluate the diagonal element (4) we need, then, retain only the $m=0$ term in the summation over m of (6) and

$$\langle M_s|\bar{V}_l(\mathbf{S})|M_s\rangle=A_l^0(\mathbf{h})\langle M_s|\bar{Y}_l^0(\mathbf{S})|M_s\rangle = N_{l0}A_l^0(\mathbf{h})\bar{P}_l(M_s)\,, \tag{8}$$

where $\bar{P}_l(M_s)$ is the operator equivalent of $P_l(z)$, with M_s substituted for z.[24] We may obtain $N_{l0}A_l^0(\mathbf{h})$ by reference to the classical potential $V_l(\boldsymbol{\alpha})$ of Eq. (5) for the special case $\boldsymbol{\alpha}=\mathbf{h}$. We note that the components of $\mathbf{h}$ in the (x,y,z) frame are, by definition, (0,0,1) and that the $Y_l^m(x,y,z)$ have the property

$$Y_l^m(0,0,1)=0, \quad \text{if } m\neq 0.$$

We can therefore write

$$V_l(\mathbf{h})=A_l^0(\mathbf{h})Y_l^0(0,0,1) =A_l^0(\mathbf{h})N_{l0}P_l(1)=A_l^0(\mathbf{h})N_{l0}\,, \tag{9}$$

since $P_l(1)=1$ for all l. Substituting (9) into (8) we obtain

$$\langle M_s|\bar{V}_l(\mathbf{S})|M_s\rangle=\bar{P}_l(M_s)V_l(\mathbf{h}). \tag{10}$$

[24] $\bar{P}_l$ is related to the commonly used unnormalized operators O_l^0 as follows: $O_2^0=2\bar{P}_2$, $O_4^0=8\bar{P}_4$, $O_6^0=16\bar{P}_6$ (see Ref. 23).

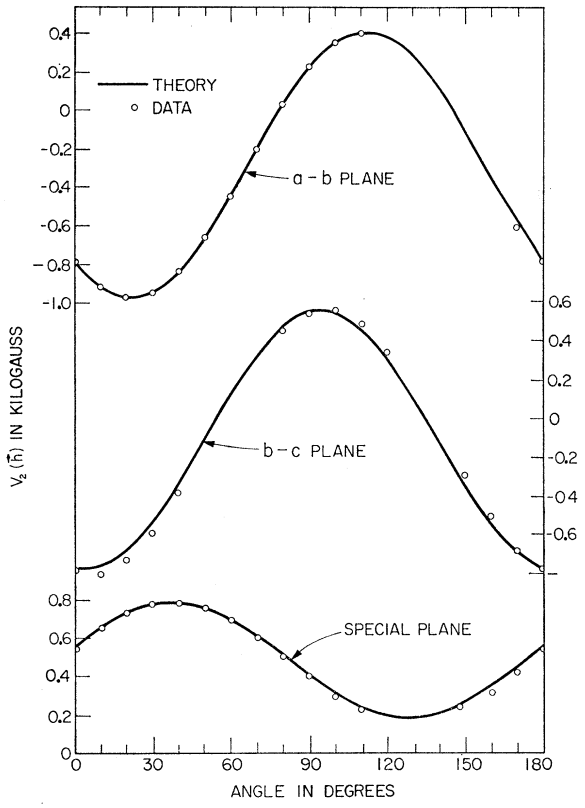

FIG. 8. Plot of the potential V_2 as a function of angle for Fe^{3+} in $YAlO_3$. The curves can be regarded as cuts of the quadratic anisotropy surface at the indicated planes. The angle is measured from the b, b, and c axes in the a–b, b–c and special planes, respectively.

The diagonal element of $\bar{V}_l$ is therefore a product of two terms: the first, $\bar{P}_l(M_s)$, is a function solely of the quantum number M_s, is fixed for a given $|S, M_s\rangle$ state, and is not a function of orientation. The second, $V_l(\mathbf{h})$, contains the angular variation of the element, and is none other than the classical equivalent of $\bar{V}_l(\mathbf{S})$. The functional form of $V_l(\mathbf{h})$ can therefore be completely determined from the angular dependence of $\langle M_s|\bar{V}_l(\mathbf{S})|M_s\rangle$.

In order to extract $\langle M_s|\bar{V}_l|M_s\rangle$ from the experimental data one must first eliminate the contribution from off-diagonal terms. If one reverses the signs of M_s and M_s' in (3) one finds

$$W(-M_s)=-g\beta HM_s+\langle M_s|\mathcal{H}_a|M_s\rangle - \sum_{M_s'=M_s}\frac{|\langle M_s|\mathcal{H}_a|M_s'\rangle|^2}{g\beta H_0(M_s-M_s')}, \quad (11)$$

and hence the sum $W(M_s)+W(-M_s)$ is to first order independent of the off-diagonal terms. In practice, since H is varied while ν is kept constant, this elimination is accomplished by subtracting from each other equations relating to opposite transitions, e.g., $(\frac{3}{2}\rightarrow\frac{5}{2})$ from $(-\frac{5}{2}\rightarrow-\frac{3}{2})$. The result, after substituting (4) and (10) into (3) and (11) is given by

$$2\sum_l V_l(\alpha)[\bar{P}_l(M_s)-\bar{P}_l(M_s-1)] = H\{-M_s\rightarrow(-M_s+1)\} - H\{(M_s-1)\rightarrow M_s\}, \quad (12)$$

where $H\{\ \}$ represents the magnetic field for which the transition indicated inside the brackets will occur at the fixed operating frequency ν. There is one such equation for each value of M_s, $1\leq M_s\leq S$. The number of equations exactly equals the number of different l. Equation (12) can therefore always be solved to give the potentials V_l directly in terms of the measured resonance fields. Solutions of Eq. (12) for $S=\frac{5}{2}$ and $S=\frac{7}{2}$ are given below in Eqs. (13) and (18), respectively.

The complete procedure can now be summarized as follows. For a given orientation $\mathbf{h}$, the resonance fields are determined for the various transitions. The values of these fields are introduced into the solutions of Eq. (12) [e.g., Eqs. (13) and (18) below], yielding experimental values of $V_l(\alpha)$ for $\alpha=\mathbf{h}$. $V_l(\alpha)$ is then plotted as a function of magnetic-field orientation and the curves are fitted to an analytic expression having the form of a harmonic polynomial of order l in α_1, α_2, α_3. The method of operator equivalents then allows one

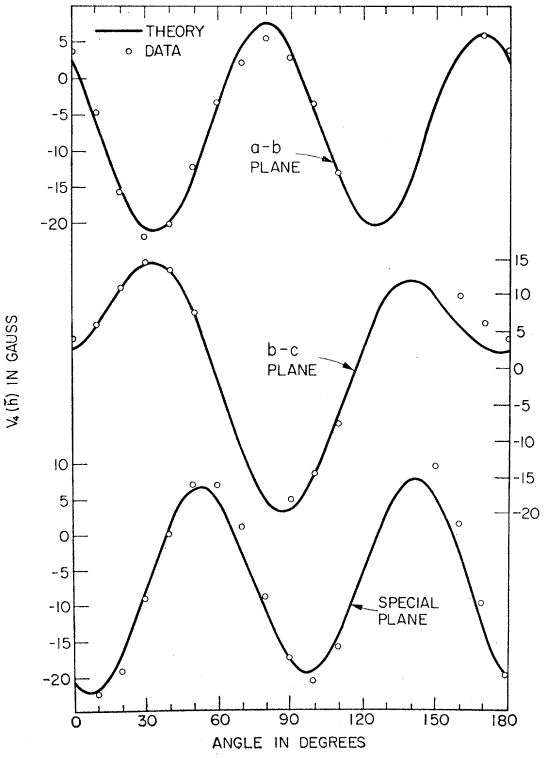

FIG. 9. Plot of the potential V_4 as a function of angle for Fe^{3+} in $YAlO_3$. The angle is measured from the b, b, and c axes in the a–b, b–c and special cuts, respectively.

to determine uniquely the form of the operators $\mathbf{V}_l(\mathbf{S})$ and thus the complete form of the spin Hamiltonian.

V. THE Fe^{3+} SPECTRUM

There are five first-order allowed transitions, namely $(-\frac{5}{2}\rightarrow\frac{3}{2})$, $(-\frac{3}{2}\rightarrow-\frac{1}{2})$, $(-\frac{1}{2}\rightarrow\frac{1}{2})$, $(\frac{1}{2}\rightarrow\frac{3}{2})$, and $(\frac{3}{2}\rightarrow\frac{5}{2})$, and we shall denote the corresponding resonance field by H_1, H_2, H_3, H_4, and H_5, in the given order. Equation (12) can be solved for V_2 and V_4, to give

$$V_2(\boldsymbol{\alpha})=(1/84)[5(H_1-H_5)+4(H_2-H_4)], \quad (13)$$

$$V_4(\boldsymbol{\alpha})=(1/210)[(H_1-H_5)-2(H_2-H_4)]. \quad (14)$$

Empirical values of $V_2(\boldsymbol{\alpha})$ derived from Figs. 3, 4, and 5 are plotted in Fig. 8: the theoretical curves represent a surface of the form

$$V_2(\boldsymbol{\alpha})=D(\alpha_3^2-\tfrac{1}{3})+E(\alpha_1^2-\alpha_2^2),$$

where D, E and the orientation of the (1,2,3) axes were chosen for best fit. The assigned values are $D=-1.45$ kOe and $E=0.30$ kOe. The orientation of the principal axes is given by the transformation

$$\begin{bmatrix}\mathbf{e}_1\\ \mathbf{e}_2\\ \mathbf{e}_3\end{bmatrix}=\begin{bmatrix}-0.570 & 0.231 & 0.788\\ 0.730 & -0.295 & 0.616\\ 0.375 & 0.927 & 0\end{bmatrix}\times\begin{bmatrix}\mathbf{e}_a\\ \mathbf{e}_b\\ \mathbf{e}_c\end{bmatrix}, \quad (15)$$

where the $\mathbf{e}_i$ represent unit vectors along the axes specified. The fit is excellent.

The term in the spin Hamiltonian which is quadratic in the spin is thus given (in kilooersted) by

$$\bar{V}_2(\mathbf{S})=-1.45[S_3^2-\tfrac{1}{3}S(S+1)]+0.30[S_1^2-S_2^2],$$

relative to principal axes given by (15).

The fourth-order surface $V_4(\boldsymbol{\alpha})$ is represented in Fig. 9. In general, the theoretical surface would contain 9 adjustable parameters. However, since the environment of the Fe^{3+} retains, in spite of some distortions, a high degree of octahedral symmetry, it was decided to attempt a fit to an octahedral potential of the form

$$V_4(\boldsymbol{\alpha})=\tfrac{1}{6}a[\alpha_\xi^4+\alpha_\eta^4+\alpha_\zeta^4-\tfrac{3}{5}].$$

A best fit was obtained for $a=-350$ Oe, and principal axes defined by

$$\begin{bmatrix}\mathbf{e}_\xi\\ \mathbf{e}_\eta\\ \mathbf{e}_\zeta\end{bmatrix}=\begin{bmatrix}0.808 & -0.574 & 0.122\\ 0.565 & 0.819 & 0.122\\ -0.174 & -0.052 & 0.985\end{bmatrix}\times\begin{bmatrix}\mathbf{e}_a\\ \mathbf{e}_b\\ \mathbf{e}_c\end{bmatrix}. \quad (16)$$

The fit, while not perfect, indicates that V_4 is still by and large octahedral in character. The term in the Hamiltonian which is 4th order in the spin, is accordingly, in oersteds,

$$\bar{V}_4(\mathbf{S})\cong-(350/6)[S_\xi^4+S_\eta^4+S_\zeta^4-\tfrac{1}{5}S(S+1)(3S^2+3S-1)].$$

The negative value of a is in contradiction with the general conclusions of Watanabe[25] and of Geschwind[26] on the sign of a for Fe^{3+} in octahedral coordination, but the experimental evidence seems conclusive in this case.

It is interesting to compare the axes of the octahedral potential with the radius vectors of the ligating oxygens. The orthogonal (rotational) part of the transformation relating the oxygen ligand system for a particular Fe^{3+} site to the crystalline frame is given by the matrix

$$\begin{bmatrix}0.781 & -0.614 & 0.122\\ 0.580 & 0.796 & 0.174\\ -0.203 & -0.064 & 0.982\end{bmatrix}. \quad (17)$$

The deviation between the two frames is less than 3°. This provides unambiguous site identification in the spectrum.

Because of the magnitude of the anisotropy energy the g factor can be determined only to an accuracy of about 1.5%. Within these limits there is no indication of anisotropy or of deviation from the g value for a free electron.

VI. THE Gd^{3+} SPECTRUM

There are seven first-order allowed transitions, namely $(-\frac{7}{2}\rightarrow-\frac{5}{2})$, $(-\frac{5}{2}\rightarrow-\frac{3}{2})$, $(-\frac{3}{2}\rightarrow-\frac{1}{2})$, $(-\frac{1}{2}\rightarrow\frac{1}{2})$, $(\frac{1}{2}\rightarrow\frac{3}{2})$, $(\frac{3}{2}\rightarrow\frac{5}{2})$, and $(\frac{5}{2}\rightarrow\frac{7}{2})$. We denote the corresponding resonance fields by H_1, H_2, H_3, H_4, H_5, H_6, and H_7 in the given order. Equation (12) can be solved for V_2, V_4, and V_6 to give

$$V_2(\boldsymbol{\alpha})=(1/252)[7(H_1-H_7)+8(H_2-H_6)+5(H_3-H_5)],$$

$$V_4(\boldsymbol{\alpha})=(1/4620)[7(H_1-H_7)-6(H_2-H_6)-9(H_3-H_5)],$$

$$V_6(\boldsymbol{\alpha})=(1/20\,790)[(H_1-H_7)-4(H_2-H_6)+5(H_3-H_5)]. \quad (18)$$

The spectra of Figs. 6 and 7 were processed to yield the angular forms of V_2, V_4, and V_6. The magnitude of V_6 was below experimental scatter, and its information could not be regarded as meaningful. V_2 and V_4 are represented in Figs. 10 and 11. The gadolinium site has reflection symmetry about the $(a-b)$ plane. The crystalline c axis is therefore a principal axis for V_2 as well as for V_4. V_2 is fit to

$$V_2=D(\alpha_c^2-\tfrac{1}{3})+E(\alpha_1^2-\alpha_2^2),$$

where

$$D=100 \text{ Oe},$$

$$E=-350 \text{ Oe},$$

and where the (1,2) axes are obtained from the $(a-b)$ axes by a clockwise rotation of 28° about the $+c$ direction. This set of axes bears no obvious relationship to the rather severe local distortions at the rare-earth site.

[25] H. Watanabe, Progr. Theoret. Phys. (Kyoto) **18**, 405 (1957).
[26] S. Geschwind, Phys. Rev. **121**, 363 (1961).

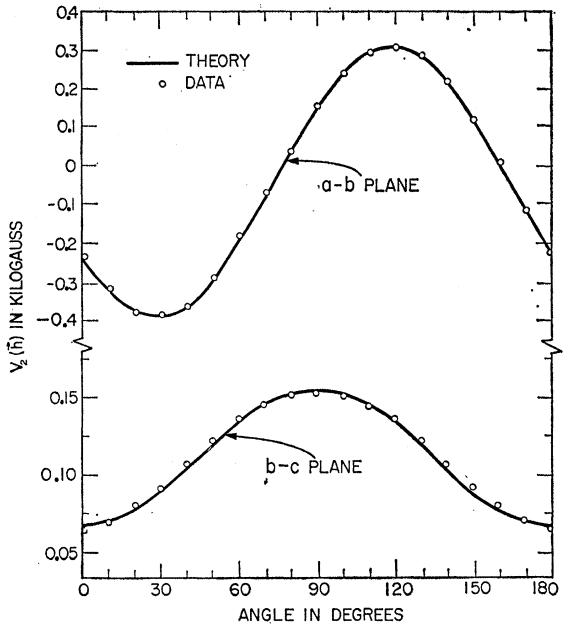

FIG. 10. Plot of the potential V_2 as a function of angle for Gd^{3+} in $YAlO_3$. The angle is measured from the a and c axes in the a–b and b–c planes, respectively.

The most general form for V_4 is

$$V_4(\alpha)=a(35\alpha_c^4-30\alpha_c^2+3)+4b(\alpha_a^2-\alpha_b^2)(7\alpha_c^2-1)+8c\alpha_a\alpha_b(7\alpha_c^2-1)+2d(\alpha_a^4+\alpha_b^4-6\alpha_a^2\alpha_b^2)+8e\alpha_a\alpha_b(\alpha_a^2-\alpha_b^2),$$

with the operator equivalent

$$V_4(S)=a[35S_c^4-30S(S+1)S_c^2+25S_c^2-6S(S+1)+3S^2(S+1)^2]+b\{(S_+^2+S_-^2)[7S_c^2-S(S+1)-5]+\text{H.c.}\}-ic\{(S_+^2-S_-^2)[7S_c^2-S(S+1)-5]-\text{H.c.}\}+d(S_+^4+S_-^4)-ie(S_+^4-S_-^4),$$

where $S_\pm=S_a\pm iS_b$, and where H.c. represents the Hermitian conjugate of the preceding expression. The coefficients a, b, c, d, and e are adjustable constants.

In the a-b plane

$$V_4(\alpha)=3a-4b\cos2\phi-4c\sin2\phi+2d\cos4\phi+2e\sin4\phi,$$

where ϕ is the angle between H and the a axis, and in the b-c plane

$$V_4=\tfrac{3}{8}(3a-4b+2d)+\tfrac{1}{2}(5a-4b-2d)\times\cos2\theta+\tfrac{1}{8}(35a+28b+2d)\cos4\theta,$$

where θ is the angle between H and the c axis. A best fit is obtained for

$$a=-0.12\text{ Oe},$$
$$b=\ 0.05\text{ Oe},$$
$$c=\ 0.24\text{ Oe},$$
$$d=\ 0.27\text{ Oe},$$
$$e=-0.30\text{ Oe}.$$

The fit is fair or good, but not excellent. Since V_4 represents a very small contribution to the present spectrum and is obtained by subtraction of large, nearly equal, magnitudes, this is not unexpected.

One may note that in a site of cubic symmetry one would expect $b=c=0$ and $a=\frac{2}{5}(d^2+e^2)^{1/2}$. It is obvious that these relations do not hold even approximately. This indicates that the rare-earth site in the orthoaluminate is so severely distorted from the cubic prototype that no visible cubicity remains. Calculation of the crystal-field effects based on a cubic approximation would appear invalid.

A comparison of the gadolinium spin Hamiltonian with that of iron, shows that (a) in the former the preponderance of the quadratic term is much more pronounced and (b) the cubic symmetry of the fourth-order term is no longer apparent. This behavior is consistent with the character of the local distortion of the oxygen atoms. A substantial component of this distortion consists of a rigid rotation of the oxygen octahedron about the iron sites. The nonrotational part of the distortion is much more severe at the rare-earth site and in fact reduces the coordination number from 12 in the ideal perovskite to an effective coordination number 9.[6]

VII. DISCUSSION: RELATION TO CRYSTAL FIELDS AND TO THE ORTHOFERRITE PROBLEM

The state of crystal-field theory is not advanced to the point where the magnetic properties of a given ion can be completely calculated from the crystal structure. This is especially true of S-state ions, where in order to account for the magnetocrystalline anisotropy it is necessary to invoke high-order compound mechanisms involving joint action of the crystal field and the spin-orbit interaction. There are nonetheless certain correlations we may expect between the crystal field present at an ion and the spin Hamiltonian. First, they

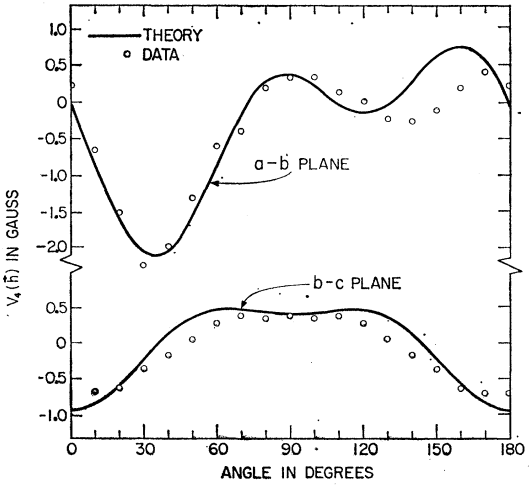

FIG. 11. Plot of the potential V_4 as a function of angle for Gd^{3+} in $YAlO_3$. The angle is measured from the a and c axes in the a–b and b–c planes, respectively.

must have the same symmetry. Secondly, we may expect the crystal field and the anisotropy surfaces $V_l(\alpha)$ of Sec. IV to have certain topological similarities.

The dominant term in $\mathcal{H}_a(\mathbf{S})$ for S-state ions is usually that quadratic in the spin coordinates. Such a quadratic form can always be diagonalized, that is, a coordinate frame $\mathbf{e}_1$, $\mathbf{e}_2$, $\mathbf{e}_3$ can be found such that

$$V_2(S)=\sum_{\mu=1} D_\mu S_\mu^2.$$

The D_μ are the principal values of the quadratic form. For Fe^{3+} in $YAlO_3$ the orientation of the $\mathbf{e}_\mu$ is not prescribed by symmetry considerations and must be determined from the data. This was done in Sec. V and the direction cosines of $\mathbf{e}_1$, $\mathbf{e}_2$, and $\mathbf{e}_3$ in the crystal unit cell frame are given by the rows of the transformation matrix of Eq. (15) of that section. The associated principal values of the D_μ are $D_1=0.78$, $D_2=0.10$, and $D_3=-0.97$ kOe.

Let us now calculate the portion of the electrostatic crystal-field potential at the Fe^{3+} ion which is quadratic in the coordinates [and hence corresponds in some way to $V_2(\alpha)$]. Unfortunately, we do not have the detailed ion position parameters for $YAlO_3$; we do, however, have them for the structurally similar $GdFeO_3$.[6] Using the ion position parameters for $GdFeO_3$, and including the effects of nearest-neighbor oxygens, and of next-nearest Fe^{3+} (or Al^{3+}) and Gd^{3+} (or Y^{3+}) ions, we obtain the potential, in unit cell frame coordinates

$$V_{c,2}=V_{20}(-5.17x^2+0.13y^2+5.03z^2 -4.20xy-0.40yz+5.60xz),$$

where various constants have been lumped into V_{20}, whose exact definition is immaterial since we are interested primarily in the topology of the quadratic form. The quadratic form is diagonalized by the coordinate transformation

$$\begin{bmatrix}\mathbf{e}_1\\ \mathbf{e}_2\\ \mathbf{e}_3\end{bmatrix}=\begin{bmatrix}0.886 & 0.283 & -0.334\\ -0.246 & 0.953 & 0.149\\ 0.387 & -0.128 & 0.910\end{bmatrix}\begin{bmatrix}\mathbf{e}_a\\ \mathbf{e}_b\\ \mathbf{e}_c\end{bmatrix},$$

with the principal values $\lambda_1=-6.45$, $\lambda_2=0.08$, and $\lambda_3=5.77$.

Though the principal values show a superficial similarity there is essentially no correlation of the spatial orientation of the ellipse corresponding to $V_2(\mathbf{S})$ that corresponding to $V_{c,2}$. It seems exceedingly unlikely that any combination of physical processes could cause the observed $V_2(\mathbf{S})$ to result from the above calculated crystal field. It is known that $V_2(\mathbf{S})$ depends sensitively on the local distortions of the host lattice from a cubic prototype, and that the distortions in $YAlO_3$ are different from those of $GdFeO_3$ (based on x-ray unit-cell dimensions). Moreover, the substitution of the somewhat large Fe^{3+} for an Al^{3+} ion must create additional distortions. Therefore, it is most probable that the crystal-field calculation above fails to correlate with the spin-resonance data because inappropriate ion position parameters have been used in the calculation. In the absence of more accurate and appropriate ion position parameters there appears to be no profit in pursuing further the crystal-field calculations of either Fe^{3+} or Gd^{3+}.

The correlation with magnetic behavior in the orthoferrites is equally poor. Assuming that the magnetic environment of the Fe^{3+} ion is similar in orthoferrite and orthoaluminate one would on the basis of the paramagnetic-resonance data, expect the ansiotropy in the former to be described by an effective field of approximately 6000 Oe along a direction close to the b axis, with a small component in the a direction. In fact, however, the iron spins are aligned in antiferromagnetic order along the a axis with slight canting towards the c axis. This suggests that the crystal fields operative in the two cases are significantly different or that the effective anisotropy in the orthoferrite is strongly exchange-dependent. In any event, the magnitude of the anisotropy interaction corroborates the conclusion of Treves[15] that one must invoke anisotropic exchange to explain the canting of the iron sublattices, since single-ion anisotropies cannot give effective canting fields large enough ($\sim 10^5$ Oe) to produce the observed magnitude of canting.

ACKNOWLEDGMENTS

The authors are indebted to Dr. Robert A. Lefever for growing the single crystals of the orthoaluminate used in these investigations, and to Dr. Kenneth A. Wickersheim for stimulating discussions of the subject matter.